ELSEVIER

Journal of Nuclear Materials 278 (2000) 1–10

journal of nuclear materials

www.elsevier.nl/locate/jnucmat

Fe–15Ni–13Cr austenitic stainless steels for fission and fusion reactor applications. I. Effects of minor alloying elements on precipitate phases in melt products and implication in alloy fabrication

E.H. Lee *, L.K. Mansur

Metals and Ceramics Division, Oak Ridge National Laboratory , P.O. Box 2008, Oak Ridge, TN 37831-6376, USA

Received 3 May 1999; accepted 13 September 1999

Abstract

In an effort to develop alloys for fission and fusion reactor applications, 28Fe–15Ni–13Cr base alloys were fabricated by adding various combinations of the minor alloying elements, Mo, Ti, C, Si, P, Nb, and B. The results showed that a significant fraction of undesirable residual oxygen was removed as oxides when Ti, C, and Si were added. Accordingly, the concentrations of the latter three essential alloying elements were reduced also. Among these elements, Ti was the strongest oxide former, but the largest oxygen removal (over 80%) was observed when carbon was added alone without Ti, since gaseous CO boiled off during melting. This paper recommends an alloy melting procedure to mitigate solute losses while reducing the undesirable residual oxygen. In this work, 14 different types of precipitate phases were identified. Compositions of precipitate phases and their crystallographic data are documented. Finally, stability of precipitate phases was examined in view of Gibbs free energy of formation.

PACS: 64.75.+g; 81.30.Mh

1. Introduction

This work was carried out in the course of developing Fe–Cr–Ni base austenitic stainless steels for fission and possible fusion reactor materials applications. Historically, various alloying elements have been added to steels during fabrication to improve or control ductility, hardenability, formability, and other properties such as resistance to corrosion, oxidation, and creep [1]. For reactor applications, however, additional considerations are required for alloying to mitigate the degradation of alloys by radiation induced cavity swelling, solute segregation, creep, and radiation hardening. Currently available heavy ion and neutron irradiation data suggest that small quantities of impurities or alloying elements can have large effects on the materials' response to radiation [2,3]. In particular, it has been known that while oxygen promotes cavity formation [4,5], fine carbide, phosphide, and silicide particles associated with Ti, C, P, and Si additions suppress cavity growth by trapping and dispersing gas atoms at particle–matrix interfaces (i.e., MC, M_2P, radiation induced γ') [6–8]. Therefore, it is important to minimize residual oxygen and to maintain certain precipitate forming elements to desired levels during alloy fabrication. Moreover, in the presence of excessive oxygen, the crucial alloying elements such as Ti, C, and Si form oxides, and their efficacy as carbide or silicide forming agents diminishes, although they appear to be present in alloys in chemical analysis. Therefore, it is

* Corresponding author. Tel.: +1-423 574 5058; fax: +1-423 574 0641.
E-mail address: LeeEH@ornl.gov (E.H. Lee).

0022-3115/00/$ - see front matter
PII: S0022-3115(99)00234-2

important to ensure that required alloying elements are maintained to desired levels and kept in an active state or in solution during alloy fabrication. With this objective in mind, a set of 28Fe–15Ni–13Cr base alloys were fabricated. Effects of alloying elements on precipitate phase stability and their impact on the final alloy compositions were systematically investigated. Finally, based on thermodynamic considerations, a proper alloy melting procedure, which facilitates the control of solute concentrations, is described. The same set of alloys was aged at 600°C and 675°C to study thermal effects in Part II (this issue), and also irradiated by heavy ions in Part III (this issue) and neutrons to investigate alloy responses to irradiation. Some of the ion and neutron data were reported previously in Refs. [9,10], respectively.

2. Alloy fabrication and characterization

A ternary Fe–15Ni–13Cr alloy was procured from Combustion Engineering, Chattanooga, Tennessee. The alloy was prepared by melting high purity electrolytic Fe, Cr, and Ni charges using argon blanked induction heating. Table 1 shows the chemical analysis of Heat No. 3756 ingot used in this study. Oxygen was a notable impurity at 0.031 wt%. From this master ternary ingot, 28 compositional variant alloys were fabricated by adding one or several alloying additions. Bars of 500 g each (13 mm × 25 mm × 130 mm) were prepared at ORNL using the non-consumable arc melting and drop casting technique. After removing hot tops, the ingots were subsequently rolled to 0.58 mm sheets having approximately 23% final cold work. A solution annealing temperature of 1200°C was applied twice during the intermediate rolling processes to assure a proper dissolution of precipitates, particularly MC particles.

During the preparation of charges, exact amounts of desired alloying elements were added to produce, in wt%, 15 Ni, 13.5 Cr, 2.2 Mn, 2.0 Mo, 0.22 Ti, 0.044 C, 0.85/0.35 Si, 0.05/0.01 P, 0.002 B, and 0.4/0.2 Nb in the final alloys. The final alloy compositions deviated somewhat from the intended compositions due to the loss of precipitates to the hot tops. The chemical compositions of the sheet alloys (not hot tops) are summarized in Tables 2 (Basic alloy series) and 3 (Engineering alloy series). In particular, oxygen analyses were carried out to confirm the exact residual oxygen contents in the final sheet alloys by using various analytical means such as vacuum fusion, calorimetric, gravimetric, and LECO T-36 (glow discharge gas analysis) methods. Of particular interest, for alloys with Ti, Si, and C additions, the residual oxygen contents in the sheets were substantially less than that in the master ternary stock. This was mainly because large fractions of light oxide and carbide particles floated up during melting and were subsequently removed with hot tops. Details will be discussed in later sections.

3. Precipitate analysis

Precipitate phases in the sheet alloys and hot tops were analyzed to understand the final alloying conditions. Precipitates were extracted by electrolytically dissolving the final sheet materials and slices from selected hot tops. Extraction was done by applying 50 mA current in 10% hydrochloric acid and 90% methyl alcohol electrolyte. Precipitate weight fractions were determined by weighing residues. The precipitate compositions were then analyzed using energy dispersive spectroscopy (EDS) techniques, and crystal structures were determined by X-ray diffraction powder method and transmission electron microscopy (TEM). When particle volume fractions were too small for X-ray analysis or particles were too thick for TEM, crystal structures were derived from the stoichiometric relationship obtained from EDS. A JEM-120CX electron microscope equipped with an energy dispersive X-ray detector was used for EDS and TEM. Details of experimental procedures were described elsewhere [11].

Fourteen precipitate phases were identified in as-fabricated alloys. Table 4 summarizes the types of precipitate phases and their weight fractions found in the sheet alloys. Table 5 summarizes crystallographic data and compositions of the precipitate phases found in all B- and E-series alloys. The precipitate weight fractions in hot tops were several-fold to an order of magnitude higher than those in the corresponding sheet alloys, suggesting that significant fractions of light oxide particles floated up during melting. Specific gravities of TiO, TiC, SiO (SiO_2 and Si mixture), CO are 4.93,

Table 1
Chemical analysis of ingot (wt%)[a]

Fe	Cr	Ni	Mo	Ti	Si	Mn	C	P	Nb	B	N	O
Bal	12.96	15.08	0.01	<0.01	0.04	<0.01	0.008	0.003	<0.01	<0.001	0.012	0.031

[a] Trace elements of S, V, Cu, Al, and Co also exist but are less than 0.01 wt%.

Table 2
Composition of B-series alloys (wt%)[a]

Alloys	Fe	Cr	Ni	Mo	Ti	Si	Mn	C	P	Nb	B	N	O
B1	Bal	13.79	14.95	–	–	–	–	–	–	–	–	–	0.030
B2	Bal	13.69	14.96	–	0.17	–	–	–	–	–	–	–	0.011
B3	Bal	13.66	15.02	–	–	0.83	–	–	–	–	–	–	0.019
B4	Bal	13.74	14.88	–	–	–	–	–	–	–	0.001	–	0.031
B5	Bal	13.68	14.94	–	0.17	–	–	0.040	–	–	–	–	0.004
B6	Bal	13.36	15.04	1.97	0.19	–	–	0.056	–	–	–	–	0.003
B7	Bal	13.55	15.01	–	0.16	0.83	–	0.041	–	–	–	–	0.004
B8	Bal	13.70	14.95	–	0.16	–	–	0.037	–	–	0.001	–	0.006
B9	Bal	13.71	15.23	–	–	–	–	–	0.049	–	–	–	0.031
B10	Bal	13.64	15.15	–	–	0.84	–	–	0.050	–	–	–	0.020
B11	Bal	13.63	15.20	–	0.18	–	–	0.041	0.049	–	–	–	0.013
B12	Bal	13.58	15.15	–	0.17	0.83	–	0.044	0.049	–	–	–	0.004
B13	Bal	13.42	14.88	–	–	–	–	0.025	–	0.40	–	–	0.005
B14	Bal	13.69	14.90	–	–	–	–	–	0.010	–	–	–	0.031

[a] Not added but showed residual impurities: <0.01Mo, <0.01Ti, <0.05Si, <0.01Mn, <0.008C, <0.004P, <0.01Nb, <0.001B, <0.015N.

Table 3
Composition of E-series alloys (wt%)[a]

Alloys	Fe	Cr	Ni	Mo	Ti	Si	Mn	C	P	Nb	B	N	O
E1	Bal	13.14	15.10	1.98	0.19	0.82	2.13	0.059	–	–	–	–	0.004
E2	Bal	13.41	14.97	–	0.19	0.80	2.16	0.055	–	–	–	–	0.003
E3	Bal	13.19	15.07	1.97	0.17	0.82	–	0.053	–	–	–	–	0.004
E4	Bal	13.21	15.11	1.98	–	0.83	2.13	0.040	–	–	–	–	0.006
E5	Bal	13.18	15.15	1.98	0.17	0.83	2.14	–	–	–	–	–	0.008
E6	Bal	13.24	15.07	1.97	0.17	0.37	2.14	0.047	–	–	–	–	0.003
E7	Bal	13.33	15.05	1.97	0.17	–	2.16	0.044	–	–	–	–	0.003
E8	Bal	13.15	15.12	1.98	0.17	0.84	2.14	0.054	0.044	–	–	–	0.004
E9	Bal	13.23	15.11	1.97	0.17	0.35	2.13	0.036	0.043	–	–	–	0.003
E10	Bal	13.30	15.08	1.98	0.18	–	2.13	0.046	0.046	–	–	–	0.004
E11	Bal	13.15	15.23	1.99	–	0.84	2.13	0.035	–	0.45	–	–	0.003
E12	Bal	13.19	15.12	1.95	–	0.35	2.12	0.023	–	0.42	–	–	0.005
E13	Bal	13.20	15.09	1.95	–	–	2.12	0.019	–	0.41	–	–	0.009
E14	Bal	13.20	15.09	1.97	0.09	–	2.15	0.044	–	0.23	–	–	0.003

[a] Not added but showed residual impurities: 0.01Mo, <0.01Ti, <0.01Si, 0.009C, <0.003P, <0.01Nb, <0.002B, <0.011N.

Table 4
Precipitate phases and their weight fractions in Fe–15Ni–13Cr base stainless steels

Alloys	Precipitate phases	Weight fraction (%)	Alloys	Precipitate phases	Weight fraction (%)
B1	Cr_2O_3	0.078	E1	TiO, TiC, MC, $Ti_{10}S_3$	0.187
B2	TiO, Ti_5S_4	0.062	E2	TiO, TiC,Ti_2S	0.225
B3	SiO[a]	0.013	E3	TiO, TiC,Ti_2S	0.167
B4	Cr_2O_3	0.062	E4	Cr_2O_3, G	0.026
B5	TiO, TiC	0.085	E5	TiO	0.107
B6	TiO, TiC	0.066	E6	TiO, TiC, $Ti_{10}S_3$	0.140
B7	TiO, TiC	0.119	E7	TiO, TiC,Ti_2S	0.114
B8	TiO, TiC	0.112	E8	TiO, TiC, MC, Ti_2S	0.032
B9	Cr_2O_3	0.092	E9	TiO, TiC	0.020
B10	SiO[a], Cr_2O_3, CrS	0.030	E10	TiO, TiC	0.082
B11	TiO, TiC, M_2P	0.107	E11	NbO, NbC, SiO[a]	0.166
B12	TiO, TiC, M_2(P, Si)	0.229	E12	NbO, NbC	0.092
B13	NbO, NbC, CrS	0.127	E13	NbO, NbC	0.085
B14	Cr_2O_3, CrS	0.072	E14	NbO, TiO, TiC	0.136

[a] SiO exists in the form of vitreous SiO_2 and Si mixture.

4.93, 2.13, 0.00125, respectively, smaller than that of Fe–Cr–Ni steels, $\simeq$8.9 g/cm^3. Analyses confirmed that precipitate phases in the hot tops were mostly oxide and carbide particles. Consequently, both the solute contents (Ti, C, Si) and the residual oxygen remaining in the sheet alloys were less than original additions.

3.1. Oxygen gettering by alloying elements

The master alloy had $\simeq$0.03 wt% residual oxygen. The residual oxygen content was reproduced in alloys B1, B4, B9, and B14, which had no Ti, C, and/or Si additions. On the other hand, alloys with Ti, C, and/or Si additions showed 30% (B3, B10) to almost 90% (B5, B6, B7, B12) reduction in residual oxygen. During melting 0.22 wt% Ti was added, but analyses showed that only about 0.17 wt% Ti was retained in the final sheet alloys. About 0.05 wt% titanium loss was accompanied by $\simeq$0.02 wt% oxygen loss in B2 alloy, indicating that titanium oxide was in the form of monoxide, TiO. The structure of TiO was confirmed by X-ray diffractometry of the extracted particles. About 0.02 wt% silicon loss was accompanied by 0.01 wt% oxygen reduction in B3 alloy, suggesting that the silicon oxide particles were in the oxygen poor monoxide form, SiO. As will be discussed later, SiO is believed to exist as a condensed mixture of vitreous SiO_2 and Si. In alloy B13, about 0.02 wt% carbon loss was accompanied by 0.023 wt% oxygen loss, suggesting that the oxygen and carbon were lost again as monoxide, CO.

About 30% oxygen reduction was observed in alloy B3, which has only Si added. About 60% oxygen reduction was observed in alloy B2 which has only Ti added. About 80% oxygen reduction was observed in alloy B13, which has C but has neither Ti nor Si. However, when both Ti and C were present together as in alloys B5, B6, B8, and B11, carbon appeared to have little effect on oxygen reduction, since oxygen reduction was accompanied by Ti reduction with little change in C concentration. Although the experimental evidence suggested that Ti was the strongest oxide former followed by C and Si, surprisingly the most efficient oxygen removal was achieved by carbon if Ti was not present. This was mainly because gaseous carbon monoxide, CO, was boiled off easily during melting. As will be discussed further, when Ti was present, TiO formation was preferred to CO, and oxygen removal efficiency was diminished because some fraction of TiO remained in the sheet alloy.

Substantial reduction of residual oxygen was also seen in alloys with Nb and C but no Ti (B13, E12, E13). The oxygen reduction was accompanied by a reduction of carbon but no appreciable niobium reduction was observed, although X-ray analyses revealed the presence of NbO and NbC particles. Specific gravities of NbO and NbC are 7.3 and 7.6 g/cm^3, respectively, close to that of the host ternary. It is thus believed that most oxygen loss occurred by CO emission and the heavy niobium oxide and carbide particles were retained in the sheet alloys.

All E-series alloys showed at least 70% reduction in residual oxygen in response to Ti, C, and/or Si additions. There was no apparent nitrogen effect on alloy compositions although there was about 0.01 wt% trace nitrogen in the master ternary. In most alloys, a few yellow diamond shaped nitride particles could be seen under an optical microscope. In the following, specific characteristics of individual precipitate phases are described.

Table 5
Characterization of thermal precipitate phases in Fe–15Ni–13Cr base austenitic stainless steels

Precipitate phases	Composition (at.%) EDS analysis	Crystal structure	Lattice parameter (nm) – X-ray	Lattice parameter (nm) – powder data	Relevant alloys (found in)
Cr_2O_3	100Cr	Hex., D_{51}, $R\bar{3}c$	$a_o = 0.4954$ $c_o = 1.3584$	$a_o = 0.4954$ $c_o = 1.3584$ card # 6-0604	Alloys with no Ti, C B1, B4, B9, B14, E4
SiO[a]	100Si	No data	Not measured	No lattice data card # 30-1127	Alloys with Si but no Ti, C B3, B10, E11
TiO	100Ti	Cubic, B1, $Fm\bar{3}m$	$a_o = 0.4251 - 0.4293$[b]	$a_o = 0.4293$ card #29-1361	Alloys with Ti
TiC	100Ti	Cubic, B1, Fm3m	$a_o = 0.4251 - 0.4293$[b]	$a_o = 0.4329$ card #6-0614	Alloys with Ti and C
TiN	Not measured	Cubic, B1, $Fm\bar{3}m$	Not measured	$a_o = 0.4246$	Alloys with Ti
MC	89Ti–11Mo 67Ti–5Cr–8Fe–20Mo 91Ti–1Cr–2Fe–6Mo	Cubic, B1, $Fm\bar{3}m$	$a_o \approx 0.4283$[b]	No data	Data from E1 and E8
NbO	100Nb	Cubic, B1, $Fm\bar{3}m$	$a_o \approx 0.4270$[b]	$a_o \approx 0.4210$	Alloys with Nb
NbC	100Nb	Cubic, B1, $Fm\bar{3}m$	$a_o = 0.4429 - 0.4461$	$a_o = 0.4470$ card #10-181	Alloys with Nb and C B13, E11, E12, E13, E14
$M_2(P,Si)$	30P–32Ti–23Cr–12Fe–3Ni 12P–20Si–27Ti–21Cr–9Fe–12Ni	Hex., C_{22}, P321	Not measured	$a_o = 0.5864$ $c_o = 0.3461$ card # 27-1171 (Fe_2P)	B11, B12
Ti_5S_4	45S–50Ti–5Cr	Not measured	Not measured	No lattice data card # 12-402	B2
$Ti_{10}S_3$	24S–62Ti–8Fe–6Mo 24S–72Ti–2Fe–2Mo	Not measured	Not measured	No data	E1, E6
Ti_2S	34Ti–66Ti	Hex.	Not measured	$a_o = 0.3206$ $c_o = 1.1190$ card # 11-664	E2, E3, E7, E8
CrS	45Cr–4Fe–4Nb–47S 47Cr–4Fe–49S	Not measured	Not measured	No data	B13, B14
G-phase	19Si–3Ti–6Cr–72Mn	Cubic, B1, $Fm\bar{3}m$	Not measured	No data	E4

[a] SiO exists in the form of vitreous SiO_2 and Si mixture.
[b] Average values due to an overlap of peaks with similar such lattice parameters from TiO, TiC and NbO.

3.2. Identification of precipitates

Chromium oxide (Cr_2O_3) precipitates were found as large spherical particles, often larger than 3 μm. Composition measured by EDS showed 100% chromium, excluding oxygen which, although present, could not be measured by EDS because of the limitations of the instrument used. X-ray diffractometry confirmed a hexagonal structure consistent with the ASTM Powder Data File of Cr_2O_3. The chromium oxide particles were found mainly in alloys B1, B4, B9, B10, and E4 which lack Ti and/or C, suggesting that Ti and C are stronger oxide former than Cr.

Silicon oxide (SiO, an intimate mixture of vitreous SiO_2 and Si) particles were present in almost perfect spherical shapes, a typical morphology of high temperature melting products. Silicon oxide particles were found in alloys with Si but no Ti or C. Particle sizes ranged from a few tenths of nanometer to a few micrometers. EDS analysis showed 100% silicon, again not counting oxygen due to the detection limitation. As mentioned already, however, the stoichiometry derived from oxygen and silicon losses indicated that the atomic ratio of Si and O in the particles is approximately equal to one ($Si/O \approx 1$). X-ray analysis did not show any discernible peaks from these particles, and thus the crystal structure of these particles could not be determined. Gibbs free energy of formation (Fig. 1, data from [12]) indicates that SiO may form initially as gas phase at high temperatures (>2000 K), but being unstable dissociates into a mixture of vitreous SiO_2 and Si as it condenses [13]. SiO is listed as a solid phase having a melting point greater than 1702°C in the CRC Handbook of Chemistry and Physics. However, the ASTM Powder Data (Card #30-1127) for SiO did not record its crystallographic information, perhaps due to the amorphous nature of the mixture.

Since both titanium monoxide (TiO) and titanium carbide (TiC) have the same $Fm\bar{3}m$ space group cubic crystal structure and very similar lattice parameters, it was difficult to distinguish them using X-rays alone. EDS also showed 100% Ti for both phases, excluding oxygen or carbon. These melt-products of titanium were generally much larger in size compared to MC particles that precipitate at lower temperatures, as described below. X-ray diffraction showed peaks of $Fm\bar{3}m$ space group crystal structure. However, the peak widths were broader than usual due to superposition of peaks from TiO and TiC phases. The average lattice parameters measured were in the range of 0.4251–0.4293 nm, close to or smaller than the lattice parameters recorded in the ASTM Powder data for both TiO (0.4293 nm) and TiC (0.4329 nm). The deviations suggest that perhaps TiO and TiC particles are non-stoichiometric.

Although it will be described further in Part II and III of this issue, here it should be pointed out that TiC, TiO, TiN, NbC, NbO, all share the same crystal structure, have similar lattice parameters, and have a capacity to

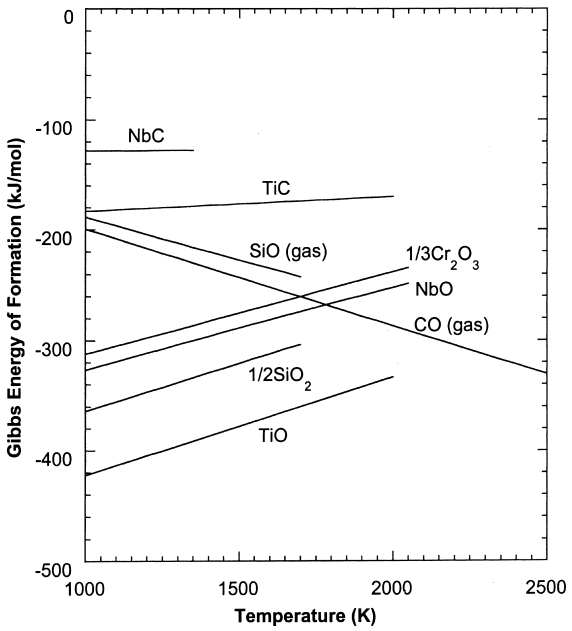

Fig. 1. Gibbs free energy of formation [12] as a function of temperature for various precipitate phases.

accommodate alloying elements such as Cr, Fe, and Mo. Therefore these phases generally occur in a complex form of (Ti, Nb, Mo, Fe, Cr) · (C, N) whenever these constituent elements are present. Such precipitate phases are often designated as MC. X-ray analyses indicated that two distinct peaks appeared when carbide and oxide phases were present together, hinting that oxygen partition in MC phase would be minimal if present, and oxide particles were likely to exist as a separate phase. In the alloys investigated in this work, most Nb containing alloys did not include Ti. In such cases, the precipitate phases are identified as NbC (instead of MC) or NbO although they may include other elements.

In the E-series alloys containing Mo, Ti, and C, EDS confirmed that there were also various Mo-rich titanium carbides (MC) in addition to the pure Ti particles (TiC, TiO) mentioned above. The latter particles were generally smaller in size, suggesting that these particles formed at lower temperatures during the cooling process. X-ray diffraction confirmed $Fm\bar{3}m$ space group crystal structure for MC particles extracted from E1 alloy. The diffraction peaks were split due to peak overlaps, suggesting that MC, TiO, and TiC phases were all present together. The MC, TiO, and TiC phases have the same crystal structure and very similar lattice parameters. The average lattice parameter of these particles was about 0.4283 nm.

All niobium containing alloys showed very irregularly shaped Nb-rich particles. Particle sizes varied from a few tenths of nanometers to several micrometers. EDS analysis showed the composition of these particles was mostly Nb, occasionally with small quantities of Fe and/or Cr. X-ray diffraction showed double peaks due to the overlap of NbC and NbO peaks, but the NbC peak intensities were an order of magnitude larger than those of NbO. Although X-ray powder data did not reveal the structure type of NbO, the parallel nature of the NbC and NbO peaks suggests that NbO has the same $Fm\bar{3}m$ space group cubic crystal structure as NbC. Although NbO phase is known to exist in two types of space group, $Fm\bar{3}m$ and $Pm\bar{3}m$, the lattice parameter measured by X-ray showed a most close match with that of $Fm\bar{3}m$ in the X-ray powder data cards.

Phosphorous-rich phases were found in all phosphorous containing alloys. Compositions of the particles varied considerably but showed approximately an M_2P stoichiometric relation. In establishing the stoichiometric relationship, the elements Ti, Cr, Fe, and Ni were considered to be in the M-sites and Si in the P-sites, after the classical work by Rundqvist [14]. The crystal structure of phosphide could not be determined because precipitate volume fractions were too small for X-ray diffraction. However, as will be shown in Part III (this issue), when the same alloys were irradiated by ions or neutrons, extensive phosphide formation occurred. In such cases, phosphide precipitates could be extracted, and the *d*-spacings matching with the hexagonal Fe_2P powder data were confirmed by TEM diffraction ring analysis.

Sulfide particles were found in various compositional and stoichiometric forms. The major constituents of sulfides were either Ti or Cr with small quantities of Fe, Mo, and Nb. Since sulfur was a trace impurity, sulfide particle number densities were extremely low. Surprisingly, among several hundreds of particles analyzed by EDS, MnS particles could not be spotted, although the formation of MnS is expected in view of thermodynamics. Since most sulfides were found to be in the form of Ti_xS_y, MnS formation appeared to be suppressed in the presence of titanium. Approximate stoichiometric relations derived from EDS analyses are summarized in Table 5.

A few unidentifiable precipitate phases were also present. One of them was a Mn-rich silicide phase having a typical composition of 19Si–3Ti–6Cr–72Mn in atomic percent. This phase was tentatively identified as G-phase, considering that the manganese fraction is similar to that in Th_6Mn_{23} type G-phase with $Fm\bar{3}m$ cubic crystal structure. Yellowish diamond or square shaped particles were observed under optical microscopy examination, particularly for Ti-containing alloys. These particles are believed to be titanium nitride based on their color and morphology. No X-ray confirmation was made because of their small volume fractions.

4. Thermodynamic considerations

Chemical analyses revealed that there was a clear correlation between alloying elements and the residual oxygen contents in the final sheet alloys. The evidence indicated that the oxide forming efficacy decreased in the order of titanium, carbon, silicon, and chromium. However, carbon acted as the most efficient oxygen remover if Ti was not present. This is because the gaseous CO boiled off easily from the system. Most oxide particles were found to be in oxygen poor monoxide forms such as TiO, CO, and SiO (a mixture of amorphous SiO_2 and Si) instead of TiO_2, CO_2, and crystalline SiO_2, perhaps due to the low oxygen levels (<0.03 wt%) in the alloys. The results, however, showed that the oxide forming trends were consistent with Gibbs free energies of formation. Empirical relations of the standard Gibbs free energies of formation (ΔG_f° in J/mol) at a given oxygen level are shown below for TiO, CO (gas), SiO (gas), SiO_2, NbO, Cr_2O_3, TiC, and NbC phases [12].

$Ti + 1/2O_2 \rightarrow TiO$	$\Delta G_f^\circ = 511\,703 + 89.12T$	600–2000 K
$C + 1/2O_2 \rightarrow CO$	$\Delta G_f^\circ = 111\,713 - 87.65T$	298–2500 K
$Si + O_2 \rightarrow SiO_2$	$\Delta G_f^\circ = 902\,070 + 173.64T$	700–1700 K
$SiO_2 + Si \rightarrow 2SiO$	$\Delta G_f^\circ = 709\,606 + 53.97T \log T - 520.07T$	298–1700 K
$Si + 1/2O_2 \rightarrow SiO$	$\Delta G_f^\circ = 96\,232 + 26.99T \log T - 173.22T$	700–1700 K
$2/3Cr + 1/2O_2 \rightarrow 1/3Cr_2O_3$	$\Delta G_f^\circ = 386\,589 + 74.27T$	298–2100 K
$Nb + 1/2O_2 \rightarrow NbO$	$\Delta G_f^\circ = -415\,68024.06T \log T + 161.08T$	298 K
$Ti + C \rightarrow TiC$	$\Delta G_f^\circ = 182\,862 + 10.01T$	298–1155 K
	$= 186\,606 + 13.22T$	1155–2000 K
$Nb + C \rightarrow NbC$	$\Delta G_f^\circ = 130\,122 + 1.67T$	1180–1370 K

Gibbs free energies were plotted as a function of temperature for the above equations in Fig. 1. In agreement with the experimental observations, TiO has the lowest Gibbs free energy of formation within the temperature range of interest, suggesting that TiO would be the most stable phase among them. Although carbon alone acted as the most efficient oxygen removing agent, its oxygen removing capacity was diminished in the presence of titanium because TiO formation became preferred over CO, and TiO particles could not be removed as easily as CO. Formation of chromium oxide was suppressed in alloys with Ti, C , and Si as expected, particularly at high temperatures.

When both carbon and oxide forming elements were present (i.e., NbC vs. NbO or TiC vs. TiO), carbide particles appeared to be more abundant than oxide particles despite the higher ΔG_f° for carbide phase. In general, carbide formation is very fast. In our customary thermal aging process, it was found that carbide formation occurred in less than a minute at 600°C. These fast kinetics might have been responsible for the preponderant carbide. Besides, in the presence of carbon, oxygen concentration was lowered by the loss of CO during alloy melting, which made the oxide formation unfavorable. In fact, the oxygen concentration in B13 alloy was reduced to 0.005 wt% from 0.03 wt% of B1 master ternary. This could have made NbO formation unfavorable because of the depletion of the needed constituent solute.

5. Conclusions

Twenty-eight Fe–15Ni–13Cr base alloys were prepared by adding various alloying elements. Fourteen different types of precipitate phases were identified. Up to four different precipitate phases were found in any one alloy, depending upon the alloy composition. The predominant precipitates were oxides, carbides, and minute amounts of phosphides, and various types of trace sulfides. Chemical analyses revealed that the final alloy compositions were noticeably affected by the formation of oxides and carbides, namely the loss of residual oxygen, Ti, C, and Si. Most losses occurred by emission of gaseous CO and by floatation of the light oxide, carbide, and silicide particles to the hot tops during melting. Although titanium was a stronger oxide former than carbon, carbon alone removed oxygen more efficiently than Ti alone, because gaseous CO molecules could be removed easily from the system. When Ti was present, TiO formation was preferred over CO. In such cases, less residual oxygen was removed because a significant fraction of solid TiO particles was retained in the system. For a similar reason, niobium alone made very little change in residual oxygen because heavy NbO particles were mostly retained in alloys. Silicon also was less efficient in removing oxygen than carbon, since a significant fraction of SiO was retained as a mixture of amorphous SiO_2 and Si.

Gibbs free energies for the oxide formation were in the order of $\Delta G_f^\circ(TiO) < \Delta G_f^\circ(CO) < \Delta G_f^\circ(SiO,\ \text{gas})$, consistent with the experimentally observed stability of these phases. However, the stability of NbC vs. NbO did not follow the trend expected from Gibbs free energy considerations. However, if oxygen levels remaining in alloys and the aspect of formation kinetics are considered, the experimental findings could be justified.

As mentioned already, it is well known that oxygen promotes cavity formation under irradiation [5,6] and that fine carbide and phosphide particles suppress cavity growth by trapping and dispersing gas atoms at their particle–matrix interfaces [7–9,15–18]. It is thus very important to minimize the impurity oxygen level and at the same time to maintain the precipitate forming elements such as Ti, C, Si, and P in solution during alloy fabrication. In this work, however, it was found that these solute elements were reduced or deactivated when oxides formed. It is important to recognize that, if alloying elements are in oxide forms, they cannot be active in carbide or silicide forming processes during irradiation. In such cases, alloys with seemingly adequate bulk compositions may not have effective matrix concentrations of desirable solutes and may not be suitable for applications to critical components of fission and fusion reactors. Fortunately however, carbon was found to act as an extremely efficient oxygen removing agent if Ti was not present. Therefore, in alloy fabrication, it is recommended to remove impurity oxygen first by melting the Fe–Cr–Ni ternary with carbon only, determine the remaining carbon level, supplement the missing portion of carbon, add desired alloying

elements, and finally fabricate alloys with conventional melting practices. Finally it should be pointed out that, as shown in Table 3, all E-series alloys with Ti or C addition have less than 0.006 wt% oxygen. This seemingly low oxygen concentration occurred, however, at the expense of Ti and/or C losses. Better alloys could have been made if oxygen were removed by carbon before adding other alloying elements.

Acknowledgements

This research was sponsored by the Division of Materials Sciences, US Department of Energy, under contract No. DE-AC05-96OR22464 with Lockheed Martin Energy Research Corporation. The authors wish to thank Drs P.J. Maziasz and S. Babu for reviewing the manuscript. Also special thanks are due to the editor, Dr H. Kleykamp, for the critical comments on the nature of silicon oxide, which was invaluable in improving the manuscript.

References

[1] F.B. Pickering, Physical Metallurgy and the Design of Steels, Applied Science, Barking, 1978.
[2] J.F. Bates, W.G. Johnston, International Conference on Radiation Effects in Breeder Reactor Structural Materials, Scottsdale, AZ, June 1977, p. 625.
[3] P.J. Maziasz, in: B.L. Bramfit, R.L. Benn, C.R. Brinkman, G.F. Vander Voort (Eds.), ASTM STP 979, American Society for Testing and Materials, Philadelphia, 1988, p. 116.
[4] E.H. Lee, L.K. Mansur, Philos. Mag. A 61 (1990) 751.
[5] S.J. Zinkle, E.H. Lee, Metall. Trans. A 21 (1990) 1037.
[6] E.H. Lee, L.K. Mansur, Metall. Trans. A 23 (1992) 1977.
[7] K. Ehrlich, K. Anderko, J. Nucl. Mater. 124 (1984) 229.
[8] K. Herschbach, W. Schneider, K. Ehrlich, J. Nucl. Mater. (1993) 233.
[9] E.H. Lee, L.K. Mansur, Philos. Mag. A 61 (1990) 733.
[10] E.H. Lee, N.H. Packan, in: N.H. Packan, R.E. Stoller, A.S. Kumar (Eds.), 14th International symposium on Effects of Radiation on Materials, vol. 1, ASTM STP 1046, American Society for Testing and Materials, Philadelphia, 1989, p. 133.
[11] E.H. Lee, P.J. Maziasz, R.F. Rowcliffe, in: J.R. Holland, L.K. Mansur, D.I. Potter (Eds.), Phase Stability during Irradiation, AIME, 1981, p. 191.
[12] O. Kubaschewski, C.B. Alcock, Metallurgical Thermochemistry, 5th Ed., Pergamon, New York, 1979.
[13] JANAF Thermochemical Tables, 2nd Ed., Office of Standard Reference Data, National Bureau of Standards, Washington, DC, 1971.
[14] S. Rundquist, Binary Transition Metal Phosphides, Arkiv För Kemi 20 (1962) 67.
[15] P.J. Maziasz, Scripta Metall. 14 (1980) 1251.
[16] A.F. Rowcliffe, E.H. Lee, J. Nucl. Mater. 108&109 (1982) 306.
[17] W. Kesternich, J. Nucl. Mater. 127 (1983) 153.
[18] E.H. Lee, L.K. Mansur, J. Nucl. Mater. 141–143 (1986) 695.